Unified model of matter-wave-packet evolution and application to spatial coherence of atom interferometers

Y. Japha*
Department of Physics, Ben-Gurion University of the Negev, Be'er Sheva 84105, Israel

(Received 30 August 2021; accepted 21 October 2021; published 10 November 2021)

We present a model that unifies Gaussian wave-packet evolution with the so-called "time-dependent Thomas-Fermi approximation" for a Bose-Einstein condensate (BEC) of strongly interacting atoms. The unified simple intuitive formalism describes the stationary or time-dependent properties of single atoms, thermal clouds, or a BEC over a wide range of interaction strengths, including intermediate interaction regimes or scenarios where both interaction regimes coexist. Excellent agreement with precise numerical calculations (Gross-Pitaevskii equations) is obtained. The model is particularly suitable for describing three-dimensional evolution in free space or in time-dependent potentials for trapping, guiding, accelerating, focusing, or splitting matter waves in interferometers. We present a unified theory of spatial coherence in matter-wave interferometers and find good agreement between analytical expressions for the evolution of the coherence length of thermal atoms or a BEC and precise numerical calculations. In addition to the insight provided by the model, it supplies a simple and useful tool for the design and performance analysis of atom interferometers with many operational parameters, where a precise numerical calculation might exhaust unrealistic calculational resources.

DOI: 10.1103/PhysRevA.104.053310

I. INTRODUCTION

Matter-wave interferometry with ultracold atoms has become a wide field of fundamental and applied research [1,2] using various techniques for splitting, recombining, and probing the interferometric phase. Coherent spatial splitting of initially trapped atoms uses light pulses (in Ramsey-Bordé [3], Raman [4–7], or Bragg [8–12] configurations), potential barriers of optical or magnetic fields [13–16], or state-dependent magnetic forces [17–19]. Many of these interferometers use free space propagation between splitting and recombination, but in some implemented or proposed interferometers the atoms propagate in guiding potentials [8,16,20–30]. In any of these schemes the most crucial factor is coherence, namely, maintaining and retrieving a well-defined phase difference between the interferometer arms. It is therefore important to precisely control not only the trajectories of the interferometer arms but also the evolution of the atomic wave packet around each trajectory.

Interferometry with a Bose-Einstein condensate (BEC) has proven to be advantageous over using thermal atomic sources [28]. However, in BEC interferometry atom-atom interactions play a major role and may be crucial for determining the coherence. In particular, these interactions determine the wave-packet evolution and hence the size of the interference pattern at the output of the interferometer and the overlap between the two wave packets of the two arms. On the other hand, these interactions are an important source of phase diffusion due to number uncertainty [31–33]. Theoretical studies of dynamical effects crucial for coherence require accurate and efficient calculation methods for the evolution of atomic wave packets over long times and distances that correctly reproduce the dependence of this evolution on atom-atom interactions. For relatively small atomic densities such dynamics can be approximated by Gaussian wave-packet evolution that may provide an efficient tool for the examination of system performance and optimization. On the other hand, in the case of a dense BEC, such a calculation would require a numerical solution of the mean-field Gross-Pitaevskii equation (GPE) [34]. In recent years efficient numerical tools have made it possible to solve problems involving the time-dependent GPE in three dimensions quickly enough to allow the application of optimal control theory to optimize the manipulation of a BEC [35]. However, for many interferometric scenarios it is still very costly in terms of computer time and expertise or even impractical to solve the GPE in three dimensions for the entire interferometric sequence, especially when such a calculation needs to be iterated many times for the purpose of design and stability analysis. For the common case of a quadratic potential, an effective approximate solution for the GPE is provided by the "time-dependent Thomas-Fermi (TDTF) approximation" [36,37]. This method starts from the static TF approximation [34] for a BEC in a harmonic trap, where the atom-atom interaction energy is assumed to be much larger than the kinetic energy, and extends it to the time-dependent domain, in which a scaling approximation is assumed for the atomic density profile.

A few analytical methods were derived to bridge between the single-atom Gaussian wave-packet theory and the TF approximation for a large BEC [38–43]. These theories were mainly applied to the static state of the atoms in a trap and some were extended to specific time-dependent situations [43], but none were employed for wave-packet propagation

*japhay@bgu.ac.il

suitable for atom interferometry. More recently, a generalization of the TDTF approximation for free space propagation to arbitrary atom-atom interaction strength was proposed [44], but failed to reproduce the coherence length of an expanding BEC for a medium interaction strength.

Recently realized Stern-Gerlach interferometers [17,18,45,46] are examples of processes that combine both interaction regimes and therefore cannot be treated over their whole sequence with previous theoretical approximations. These interferometers start with a trapped BEC whose initial properties and evolution after trap release are dominated by relatively strong atom-atom interactions. The atomic wave packet is then split and the resulting wave packets are manipulated with magnetic gradient pulses that affect their trajectory, size and phase. A critical stage in this sequence is focusing along the main propagation axis into a minimal size of about 0.2 μm and then expansion to a size that is about three orders of magnitude larger to form interference patterns with a periodicity on the order of tens of μm (see Ref. [45], in particular Fig. 10). The dynamics at the focus is dominated by position-momentum uncertainty, whose effect is not included in the TDTF approximation. Only a theory that combines both interaction regimes can describe this process. As a direct GPE calculation is not straightforward in this case due to the scale changes of a few orders of magnitude over time and over the different dimensions, we have used the unified wave-packet evolution model, whose derivation and details are presented here.

The unified theory presented here not only allows the description of processes involving both interaction limits with the same formalism, but also supplies accurate predictions for the intermediate interaction regime, as we demonstrate by comparing our results to a full numerical solution of the GPE. In a way, this work follows some ideas presented in the work by Jamison *et al.* [44], but the derivation here is more general and includes evolution in the presence of external potentials, including steady-state properties in a trap. For example, our model reproduces accurately the properties of a quasi-1D BEC in the dimensionality crossover regime and correctly accounts for the dynamic transition of a BEC into the 1D regime when it expands in a matter waveguide. Our model provides correct analytical predictions for the coherence length of an expanding BEC over all interaction regimes.

In this work we present only a few simple examples of specific physical situations to demonstrate the validity of the model. Utilizing the model for analyzing real physical results beyond the Stern-Gerlach interferometer is beyond the scope of this paper, but we believe that new insights can be gained by applying it to the analysis of experiments that were analyzed previously by full GPE calculations (e.g., [47]) or recent experiments with guided matter waves that have not yet been thoroughly compared to theory (e.g., [48]), as well as feasibility studies of guided interferometry that may benefit from a more extensive theoretical treatment (e.g., [29,30]).

The structure of the paper is as follows. We present the derivation of the model in Sec. II and then, in Sec. III, apply it to simple scenarios: steady state of a BEC in a harmonic trap, expansion of a BEC in free space or a waveguide, and quick splitting into two traps. In Sec. IV we derive analytical expressions for the contrast of an interferometer with a BEC source or a thermal source upon imperfect recombination of the two arms at the output port. This part extends the work of Roura *et al.* [49], which in turn enhances the treatment of this problem by Englert, Schwinger, and Scully [50–52] in the context of what was termed "the Humpty-Dumpty effect" in a Stern-Gerlach interferometer. Our unified approach that treats a BEC and a thermal source on the same grounds provides analytical expressions for the interferometric contrast that make use of the notions of time-dependent coherence length and momentum coherence width. In Sec. V we discuss the conclusions and provide an outlook for future applications and required improvements of the model.

II. EVOLUTION EQUATIONS

A wave packet is a coherent (pure) spatially confined state of a single particle or a BEC where all the particles (atoms) share the same single-particle wave function $\psi(\mathbf{r},t)$. Wave packets can also be used to describe a statistical mixture of many single-particle states. Here we derive the evolution equations for the parameters of a single wave packet in a potential that is smooth enough, as defined below. The major part of the next subsection is quite similar to previous derivations of the TDTF approximation, but it sets the ground for the derivation of the unified model in Sec. II B.

A. Wave-packet evolution

We start with the time-dependent GPE for a BEC with N particles ($N \gg 1$) in an external potential $V(\mathbf{r},t)$

$$i\hbar\frac{\partial\psi}{\partial t} = \hat{H}_{\mathrm{MF}}(t,\psi)\psi, \tag{1}$$

where the mean-field effective Hamiltonian is

$$\hat{H}_{\mathrm{MF}}(t,\psi) = -\frac{\hbar^2}{2m}\nabla^2 + V(\mathbf{r},t) + g\eta N|\psi|^2. \tag{2}$$

The mean-field atom-atom interaction potential is proportional to the interaction strength $g = 4\pi\hbar^2 a_s/m$ (a_s being the s-wave scattering length and m the atomic mass) and to the fraction of atoms $\eta(t)$ in occupying the wave packet when part of the total number N have been split into other wave packets or lost. The GPE reduces to the linear Schrödinger equation if there is no atom-atom scattering, for example, if there is only a single atom ($N \to 0$).

The problem can be separated into the evolution of the wave-packet center $\mathbf{R}$ and the evolution relative to the center:

$$\psi(\mathbf{r},t) = e^{i[\mathbf{P}\cdot(\mathbf{r}-\mathbf{R})+S(t)]/\hbar}\Phi(\mathbf{r}-\mathbf{R},t), \tag{3}$$

where $\mathbf{P} = m\dot{\mathbf{R}}$. By substituting Eq. (3) into Eq. (1) we obtain Newton's equations of motion for the center coordinates $\dot{\mathbf{P}} = m\ddot{\mathbf{R}} = -\nabla V(\mathbf{r})|_{\mathbf{r}=\mathbf{R}}$ and the well-known expression for the action $S(t)$ as an integral over the Lagrangian

$$S = \int_0^t dt'\left[\frac{1}{2m}\mathbf{P}(t')^2 - V(\mathbf{R}(t'),t')\right]. \tag{4}$$

The equation for $\Phi(\mathbf{r}-\mathbf{R})$ in the frame of reference moving with the center coordinates $\mathbf{R}(t)$ becomes

$$i\hbar\frac{\partial\Phi}{\partial t} = [H_{MF}(t,\Phi) - V(\mathbf{R}) - (\mathbf{r}-\mathbf{R})\cdot\nabla V(\mathbf{R})]\Phi, \tag{5}$$

such that the zeroth- and first-order terms in the expansion of $V(\mathbf{r},t)$ around $\mathbf{r}=\mathbf{R}$ are eliminated from the Hamiltonian H_{MF} in the moving frame. In this frame we approximate the potential as quadratic (the next order in the Taylor expansion around $\mathbf{r}=\mathbf{R}$):

$$V_c(\mathbf{r}-\mathbf{R},t)\approx\frac{1}{2}\sum_j Q_j(t)(r_j-R_j)^2, \tag{6}$$

where $j=x,y,z$. For simplicity we assume within the scope of this paper that the potential axes coincides with the coordinates x,y,z and does not change during the evolution. A more general case of rotating axes is discussed in the context of the TDTF approximation [37]). From here on we transform into the frame moving with $\mathbf{R}$ so that $\mathbf{R}\to 0$.

Under the quadratic condition (6) we can make the scaling ansatz [36]

$$\Phi(\mathbf{r},t)=\frac{\chi\left(\frac{x}{\sigma_1},\frac{y}{\sigma_2},\frac{z}{\sigma_3}\right)}{\sqrt{\sigma_1\sigma_2\sigma_3}}\exp\left(\frac{i}{2}\sum_j\alpha_j r_j^2+i\varphi\right), \tag{7}$$

where $\sigma_1,\sigma_2,\sigma_3$ are time-dependent parameters representing the size of the wave packet along the three Cartesian axes, and α_j and φ are functions of the size parameters (see below), such that α_j can be regarded as a momentum chirp $\alpha_j=\partial k_j/\partial r_j$ and $\varphi(t)$ is a global phase of the wave packet. The function $\chi(u,v,w)$ is assumed to be normalized,

$$\int du\int dv\int dw\,|\chi(u,v,w)|^2=1, \tag{8}$$

and can also be chosen to satisfy

$$\int du\int dv\int dw\,u^2|\chi(u,v,w)|^2=1, \tag{9}$$

and the same for v^2 or w^2 replacing u^2 in the integral. Equations (8) and (9) ensure that the wave function $\Phi(\mathbf{r},t)$ is normalized and that at any time

$$\sigma_j(t)=\sqrt{\int d^3\mathbf{r}\,r_j^2|\Phi(\mathbf{r},t)|^2} \tag{10}$$

are the sizes of the wave packet in the three Cartesian directions.

The scaling ansatz (7) was first used in the context of evolution of a BEC by Castin and Dum [36] and then by many authors (see Refs. [37,49] and references therein). The scaling approach was originally derived for a wave function satisfying the Thomas-Fermi (TF) approximation and was termed "the time-dependent Thomas-Fermi method." In this case the normalized function $\chi(u,v,w)$ is given by

$$\chi_{TF}(\rho)==\sqrt{\frac{15}{8\pi\times 7^{3/2}}}\left(1-\frac{\rho^2}{7}\right)^{1/2}_{\rho^2<7}, \tag{11}$$

for $\rho^2\equiv u^2+v^2+w^2$. For this inverted parabolic function, which represents the TF approximation for the ground state of a BEC with strong interactions in a harmonic trap, it was shown that the shape is conserved during evolution in a quadratic potential with time-dependent harmonic frequencies. On the other hand, one may note that the scaling ansatz is the exact solution for the evolution of a Gaussian wave packet in a quadratic potential in the absence of atom-atom interactions, as shown explicitly below. In this case the function χ is

$$\chi_G(\rho)=(2\pi)^{-3/2}e^{-\rho^2/4}. \tag{12}$$

However, the scaling assumption is not satisfied in the intermediate regime between these two limits. For example, consider a BEC in a tight trap, whose ground-state wave function satisfies the TF approximation and has an inverted parabolic shape χ_{TF}. If the trapping potential is reduced adiabatically the BEC wave function is expected to become the ground state of a dilute BEC with weak interactions, and its shape will become more like a Gaussian χ_G. Although in general the scaling assumption is not strictly accurate, we show in this work that the wave-packet sizes and hence some important properties of the wave packet can be continuously followed through the intermediate range between the two limits through an equation of motion that combines both of them. We therefore keep the specific shape of the wave packet implicit, leaving room for the option that χ may change in time while continuously satisfying Eqs. (8) and (9). We focus on the global properties of the wave packet that follow from the sizes σ_j.

B. Derivation of the equations of motion

By substituting the ansatz (7) into the left-hand side of Eq. (1) and into the kinetic term in Eq. (2) we obtain

$$\frac{i\dot{\Phi}}{\Phi}=-\sum_j\left(i\frac{\dot{\sigma}_j}{2\sigma_j}+\frac{ir_j\dot{\sigma}_j}{\sigma_j^2}\frac{\partial_j\chi}{\chi}+\frac{\dot{\alpha}_j}{2}r_j^2\right)-\dot{\varphi}, \tag{13}$$

$$-\frac{\hbar}{2m}\frac{\nabla^2\Phi}{\Phi}=-\frac{\hbar}{2m}\sum_j\left[\frac{1}{\sigma_j^2}\frac{\partial_j^2\chi}{\chi}+\frac{2i\alpha_j r_j}{\sigma_j}\frac{\partial_j\chi}{\chi}+i\alpha_j-\alpha_j^2r_j^2\right], \tag{14}$$

where ∂_j denotes differentiation with respect to the dimensionless argument r_j/σ_j of the function χ. By equating the terms proportional to $r_j\partial_j\chi$ in the two equations we obtain for the momentum chirp

$$\alpha_j(t)=\frac{m}{\hbar}\frac{\dot{\sigma}_j}{\sigma_j}, \tag{15}$$

where the relative expansion rate $\dot{\sigma}_j/\sigma_j$ along each axis may be interpreted as a chirp of the local velocity $\partial v_j/\partial r_j$ along the wave packet. In the original time-dependent TF theory [36] the kinetic terms $\partial_j^2\chi$ are neglected. In Ref. [44] it was suggested to replace these terms by the second derivatives of the ground-state wave function calculated by solving the steady-state GPE. Here we find it more useful to approximate these terms by

$$-\frac{\partial_j^2\chi}{\chi}\approx\frac{1}{2}\left(1-\frac{1}{2}\frac{r_j^2}{\sigma_j^2}\right). \tag{16}$$

This relation is exact if $\chi=\chi_G$ is a Gaussian and becomes less accurate with increasing interaction strength, where $\chi\to\chi_{TF}$. On the other hand, with increasing interaction this term becomes less dominant or even negligible with respect to the

interaction term. We approximate the interaction term in the GPE as in the original time-dependent TF approximation,

$$\eta g N|\Phi|^2 \approx \eta g N \frac{\chi_{TF}|^2}{\sigma_1\sigma_2\sigma_3} \equiv \mu_{\rm int}\left(1-\frac{1}{7}\sum_j \frac{r_j^2}{\sigma_j^2}\right), \tag{17}$$

where $\chi_{TF}(x/\sigma_1, y/\sigma_2, z/\sigma_3)$ is given in Eq. (11) and the last term is zero whenever it is not positive, while $\mu_{\rm int}$ can be interpreted as the interaction chemical potential. By collecting the terms proportional to r_j^2 we obtain

$$\ddot{\sigma}_j = \frac{\hbar^2}{4m^2}\left(\frac{1}{\sigma_j^3}+\frac{\eta\beta a_s N}{\sigma_j\sigma_1\sigma_2\sigma_3}\right) - \frac{Q_j}{m}\sigma_j, \tag{18}$$

where $\beta = 60/7^{5/2} = 0.4628$ psee discussion of an improved value around Eq. (32) below].

Equation (18) is the main result of this section. The first term on the right-hand side does not exist in the TDTF model and represents an effective repulsive force due to momentum-position uncertainty. The second term is the mean-field repulsive force due to atom-atom interactions, and the third term is due to the external harmonic force (if $Q_j/m = \omega_j^2 > 0$) or antiharmonic force (if $Q_j < 0$). In the absence of interactions $a_s N \to 0$, where the wave-packet envelope is a Gaussian function, Eq. (16) is exact, and hence Eq. (18) is also exact. In the opposite limit of strong interactions the first term becomes negligible, and Eq. (18) reduces to a form equivalent to the equation for the scaling factors in the TDTF approximation.

Equation (18) can be viewed as a classical equation of motion

$$m\ddot{\boldsymbol{\sigma}} = -\frac{\partial U(\boldsymbol{\sigma})}{\partial \boldsymbol{\sigma}}, \tag{19}$$

where the potential is given by

$$U(\boldsymbol{\sigma}) = \sum_{j=1}^{3}\left(\frac{\hbar^2}{8m\sigma_j^2}+\frac{1}{2}Q_j\sigma_j^2\right) + \frac{\hbar^2}{4m}\frac{\eta\beta a_s N}{\sigma_1\sigma_2\sigma_3}. \tag{20}$$

Here the first term is the "quantum potential" due to the uncertainty principle, the second term is due to the external potential, and the last term is the mean-field interaction chemical potential $\mu_{\rm int}$ [see Eq. (17)].

If the initial wave-packet sizes $\sigma_j(0)$ are the steady-state solution ($\ddot{\sigma}_j = 0$) of Eq. (18) with $\eta = 1$ and $Q_j/m = \omega_j^2$, then we can write an equivalent equation for the scaling factors

$$\lambda_j(t) \equiv \frac{\sigma_j(t)}{\sigma_j(0)}, \tag{21}$$

$$\ddot{\lambda}_j = \frac{\nu_j^2}{\lambda_j^3} + \eta\frac{\omega_j^2-\nu_j^2}{\lambda_j\lambda_1\lambda_2\lambda_3} - \frac{Q_j}{m}\lambda_j, \tag{22}$$

where

$$\nu_j = \frac{\hbar}{2m\sigma_j(0)^2}. \tag{23}$$

Equation (22) generalizes the scaling equations of the TDTF model to the case where the initial kinetic energy is not negligible and the atomic fraction η may vary. It reduces to the TDTF model if $\nu_j \to 0$ and $\eta = 1$.

Let us note that in the absence of interactions, $a_s N \to 0$, the wave-packet model with Eq. (18) can be further extended to a complete set of wave functions: the Gaussian Hermite functions

$$\chi_{\mathbf{n}}(u,v,w) = \chi_G(u,v,w)H_{n_1}(u)H_{n_2}(v)H_{n_3}(w), \tag{24}$$

where H_n are Hermite polynomials of order n. The derivation of Eq. (18) is completely valid for this family of functions in the absence of interactions, except that in Eq. (16) $1 - r_j^2/2\sigma_j^2 \to 2n_j + 1 - r_j^2/2\sigma_j^2$. This additional term does not affect Eq. (18), and the scaling ansatz is accurate for each of these functions. However, while σ_j represents the width of the Gaussian part χ_G, the actual size of the Gaussian-Hermite wave packet is $\langle r_j^2\rangle_{n_j} = \sigma_j^2(2n_j+1)$. This determines the phase φ_{n_1,n_2,n_3} of each Gaussian-Hermite wave packet, such that in a noninteracting system the evolution of an arbitrary wave function can be calculated by expanding it in Gaussian-Hermite basis functions with a common size vector $\boldsymbol{\sigma} = (\sigma_1, \sigma_2, \sigma_3)$. The state at any time is then exactly given by a superposition with the same initial coefficients and the ansatz (7) with corresponding phases calculated from the solution of Eq. (18). In the following we also use the Gaussian-Hermite set to describe the evolution of thermal clouds whose initial state can be described as a mixture of such states.

The phase φ in Eq. (7) is obtained by collecting the remaining terms in Eqs. (13) and (14), which do not depend on the coordinates, together with the coordinate independent part of the interaction term in Eq. (2). We then find

$$\dot{\varphi} = -\frac{1}{\hbar}\left[\mu_{\rm int}(t) + \sum_j \frac{\hbar^2}{2m\sigma_j^2}\left(n_j+\frac{1}{2}\right)\right], \tag{25}$$

where $\mu_{\rm int}$ is defined in Eq. (17). The first term in Eq. (25) represents the mean-field effective interaction chemical potential [see Eq. (17) and (20)], and the second term represents the internal kinetic energy at the wave-packet center, with n_j corresponding to the mode numbers if the wave packet is a Gaussian-Hermite function as in Eq. (24) and $n_j = 0$ for a regular BEC.

To conclude this section, let us describe briefly the recipe for calculating wave-packet evolution in an interferometric sequence with a time-dependent potential $V_i(\mathbf{r}, t)$ in one of the interferometer arms (denoted by the index i), provided that the potential satisfies the smoothness conditions stated after Eq. (2). One usually starts with the initial wave-packet sizes obtained from the steady-state solution of Eq. (18) in the trapping potential, as described in the next section. To calculate the evolution in three dimensions one needs to solve a set of first-order ordinary differential equations for a vector of 12 components: six values of the wave-packet center position and velocity and six values of the wave-packet sizes and their time derivatives, while the accumulating phase is obtained by integrating Eq. (25) over time. At each point in time one uses a quadratic expansion of the local potential around the instantaneous solution for the coordinates $\mathbf{R}(t)$ to obtain $Q_j(t)$. In parts of the sequence where the initial wave packet is split one must take into account the reduction of the number of particles in each arm by properly taking the parameter η, as demonstrated below in Sec. III D.

In the following we compare some of these solutions with exact numerical solutions of the GPE and derive analytical solutions for some cases where this is possible.

III. SIMPLE APPLICATIONS

In this section we present some simple applications of the unified wave-packet evolution model that demonstrate the range of its utility. By comparison with exact numerical solutions of the GPE we show that the steady-state solution of Eq. (18) provides an excellent approximation for the properties of a BEC over a wide range of atom-atom interaction strength in a harmonic trap with arbitrary frequencies. In particular, the solutions faithfully reproduce the properties of a BEC in the crossover regime between a 3D and a quasi-1D condensate. We derive general analytical expressions for the expansion and collimation of an atomic cloud in free space and a waveguide, where a unified model is essential for describing the dynamical transition from 3D to quasi-1D. Finally, we examine the effect of splitting a BEC into two trapped wave packets with half the initial number of particles in each. We compare the results of the unified model to an exact GPE solution and to other approximations and demonstrate the validity of the unified model.

A. BEC in a harmonic trap

The steady-state equations for a BEC in a harmonic trap with frequencies ω_j follow from Eq. (18) by setting $\ddot{\sigma}_j = 0$ and $Q_j = m\omega_j^2$. By defining the harmonic oscillator lengths ℓ_j as

$$\ell_j \equiv \sqrt{\frac{\hbar}{2m\omega_j}}, \tag{26}$$

we can write the steady-state equations as

$$\frac{1}{\sigma_j^4} + \frac{\beta a_s N}{\sigma_j^2 \sigma_1 \sigma_2 \sigma_3} = \frac{1}{\ell_j^4}. \tag{27}$$

In the limit of no interactions $a_s N \to 0$ the equations are uncoupled and the solution is readily given by $\sigma_j = \ell_j$. In the limit of strong interactions (the TF limit) the first term on the left-hand side is neglected, and we find

$$\sigma_j^{TF} = \frac{\ell_j^2}{\sqrt{7}\bar{\ell}}\left(\frac{60 a_s N}{\bar{\ell}}\right)^{1/5} = \frac{r_{j,\max}}{\sqrt{7}}, \tag{28}$$

where $\bar{\ell} = (\ell_1 \ell_2 \ell_3)^{1/3}$ and $r_{j,\max}$ is the TF radius—the edge of the TF wave function in each direction.

Before examining the solutions of Eq. (27) for intermediate interaction strengths, let us briefly discuss the interaction energy and chemical potential of the ground state. The chemical potential is $\mu = \hbar\dot{\varphi}$, where $\dot{\varphi}$ is given in Eq. (25), with ν_j defined in Eq. (23), $n_j = 0$, and $\mu_{\rm int}$ defined in Eq. (17) (for $\eta = 1$). The chemical potential represents the energy of a single particle in the presence of all other particles, such that in the middle of the trap, where the harmonic potential is zero, this energy consists of the kinetic energy and interaction energy. The average interaction energy is obtained by integration over the atomic density approximated in Eq. (17)

$$E_{\rm int} = gN \int d^3\mathbf{r}\, |\Phi(\mathbf{r})|^4 \approx \frac{4}{7}\mu_{\rm int}, \tag{29}$$

where the interaction chemical potential is found from Eq. (27) for the ground state to be

$$\mu_{\rm int} = \frac{7}{2} m\omega_j^2 \sigma_j^2 \left[1 - \left(\frac{\ell_j}{\sigma_j}\right)^4\right] = \frac{7\beta}{32\pi}\frac{gN}{\sigma_1\sigma_2\sigma_3}. \tag{30}$$

In the TF limit $\sigma_j \gg \ell_j$ we can substitute the expression in Eq. (28) for σ_j and obtain the well-known result (e.g., [34])

$$\mu_{TF} = \hbar\bar{\omega}\left(\frac{15 a_s N}{8\bar{\ell}}\right)^{2/5}, \tag{31}$$

where $\bar{\omega} = (\omega_1\omega_2\omega_3)^{1/3}$.

For intermediate interaction strengths the wave-packet sizes σ_j are found self-consistently by a very easy numerical solution of Eq. (27). By comparing these solutions and the resulting values of the chemical potential to the results of a numerical solution of the time-independent GPE we find a fairly good agreement—less than ±5% error over most of the range of parameters covering weak and strong interactions, except for the estimated interaction energy $E_{\rm int}$ for very weak interactions, where the deviation may reach up to 18% out of a very small value. Nevertheless, the results presented below are based on a simple procedure that improves the accuracy of the approximation. This is done by releasing the assumption that the interaction mean-field potential has the 3D inverted parabolic shape of Eq. (17). In practice, when the interactions are weak or if the aspect ratio between the trap axes is large, the wave packet may become more similar to a separable function $\chi(u, v, w) \approx \chi_1(u)\chi_2(v)\chi_3(w)$, where it may have a parabolic shape along one of the dimensions and a shape closer to a Gaussian along other dimensions. In such a case where each dimension is treated separately as a 1D problem the normalization condition gives $\beta_{1D} = 6/5^{3/2} = 0.5367$, which is larger than the 3D value $\beta_{3D} = 60/7^{5/2} = 0.4628$ given after Eq. (18) by ∼16%. A simple procedure that provides high accuracy uses interpolation between the two values,

$$\beta(\boldsymbol{\sigma}) = \beta_{3D} + (\beta_{1D} - \beta_{3D})\left\langle \frac{\ell_j^2}{\sigma_j^2}\right\rangle_{\max}, \tag{32}$$

where $\langle \ell_j^2/\sigma_j^2\rangle_{\max}$ is an average of the ratio over the two indices j where it is maximal. If $\sigma_j \gg \ell_j$ along at least two axes then $\beta \approx \beta_{3D}$, whereas if $\sigma_j \sim \ell_j$ along two axes then $\beta \approx \beta_{1D}$. The σ_j-dependent value of β is used within the self-consistent calculation of σ_j in Eq. (27) and yields more accurate solutions for σ_j in the intermediate interaction regime, allowing less than ±1% deviation from the GPE results for all the parameter ranges that were examined here.

As demonstrated in Figs. 1 and 2 for typical trap parameters, the predictions of our unified model (UM) are in excellent agreement with the numerical steady-state solutions of the GPE over the whole range between the standard TF regime (large atom number) and the weak interaction limit (small atom number). Our approximation does not provide a prediction about the exact shape of the wave function. In the inset of Fig. 1(a) we present a comparison between the density profile obtained from the GPE and the two limits of the wave-packet density profile—a Gaussian and an inverted parabola, both having the same widths σ_j as defined in Eq. (10). Although

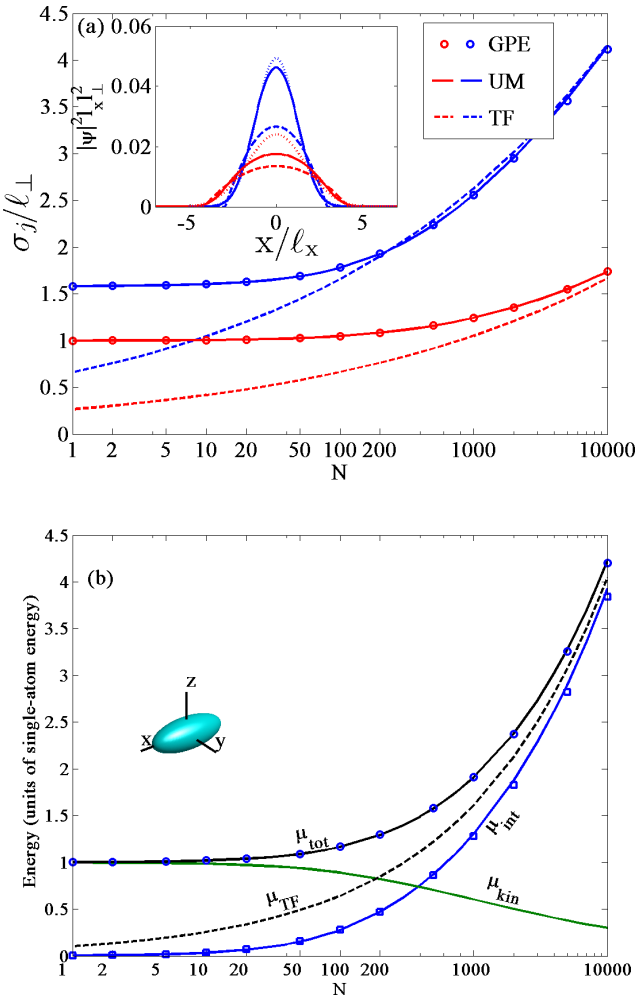

FIG. 1. Steady-state solutions of the unified model (UM) for the ground state of bosonic atoms in a harmonic trap. The UM (solid lines) is compared to a numerical solution of GPE (circles) and to standard TF approximation (dashed). The UM is shown to be accurate (within $\pm 1\%$) over the whole range of mean-field interaction strengths (number of atoms N). (a) Wave function widths σ_x (blue) and $\sigma_\perp$ (red), in units of the perpendicular oscillator length $\ell_\perp = 0.763\,\mu$m, as a function of atom number for ^{87}Rb atoms (mass $m = 1.44 \times 10^{-25}$ kg, s-wave scattering length $a_s = 5.29$ nm) in a cylindrically symmetric harmonic trap with frequencies $\omega_\parallel = 2\pi \times 40$ Hz and $\omega_\perp = 2\pi \times 100$ Hz. Inset: probability density profiles $|\Phi(x, 0, 0)|^2$ along the longitudinal trap axis: GPE result (solid) compared to an inverted parabolic [Eq. (11), dashed] and Gaussian (dotted) profile [satisfying Eq. (12)] having the same widths σ_j. For $N = 100$ (blue) the GPE profile is closer to the Gaussian, while for $N = 1000$ (red) it is intermediate between the two approximate profiles. (b) The chemical potential due to interaction $\mu_{\rm int}$ and kinetic energy $\mu_{\rm kin} = \frac{1}{2}\hbar\sum_j \nu_j$ at the trap center. The total chemical potential $\mu_{\rm tot} = \mu_{\rm int} + \mu_{\rm kin}$ according to the UM shows excellent agreement with GPE solution (circles for $\mu_{\rm tot}$ and squares for $\mu_{\rm int} = \frac{7}{4}gN\langle|\Phi|^2\rangle$). Inset: potential isosurface and definition of axes.

neither of the two limits of the density profile is close to the accurate profile in the intermediate interaction regime, the UM is still successful in providing an excellent prediction for the basic properties of the wave function: size and energy.

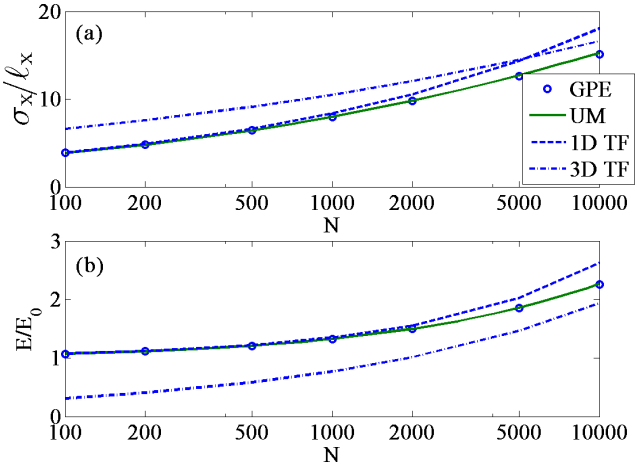

FIG. 2. Steady-state solutions of the unified model (UM) for the ground state of N bosonic atoms in an elongated trap ($\omega_y = \omega_z \equiv \omega_\perp = 2\pi \times 10$ kHz, $\omega_x = 2\pi \times 40$ Hz, other parameters as in Fig. 1). (a) The longitudinal cloud width (in units of the single-particle width $\ell_x = 1.2\,\mu$m) and (b) the ground-state chemical potential (in units of the single-particle energy $E_0 = \frac{1}{2}\hbar\sum_j \omega_j$). The UM (solid lines) agrees very well with results from a numerical solution of the GPE (circles) over the entire range, while both agree with the 1D TF approximation only for low atom numbers, where the transverse wave function is the single-particle Gaussian ground state in the transverse potential. This demonstrates the validity of the UM in predicting the transition from 3D to 1D for a BEC in elongated traps. The condensate approximation is valid throughout the range shown at zero temperature since the γ factor for transition into the Tonks-Girardeau regime is small. The 3D TF approximation is valid only for N beyond the range shown.

These steady-state predictions are therefore a good starting point for studying the time evolution of the wave packets in interferometric situations, as demonstrated below.

An important application of the UM is the transition from a 3D BEC to a quasi-1D Bose gas in an elongated trap [53–55]. In the 1D limit the large energy splitting between single-particle transverse eigenmodes of the potential allows scattering only along the longitudinal direction, and hence the atomic dynamics is limited to one dimension while the wave function in the transverse direction is fixed at the lowest eigenstate of the harmonic potential. The physics along the longitudinal axis is then governed by an effective interaction strength $g_{1D} = g/4\pi\ell_\perp^2 = 2\hbar\omega_\perp a_s$ [54]. As long as the factor $\gamma = 2m\omega_\perp/\hbar n$, where n is the 1D atomic density, is small ($\gamma \ll 1$), the condensate assumption for the many-body ground state is valid (otherwise a Tonks-Girardeau gas is formed [54,56]). As demonstrated in Fig. 2, the UM allows a fairly accurate prediction of the BEC properties over a broad range of parameters starting with a fully 1D BEC for low atom numbers (weak interaction) through the transition to a 3D BEC, where the interaction is strong enough to become dominant in the transverse direction. We emphasize that, beyond its simplicity, the main advantage of our unified model over previous models used to predict the properties of the ground state of a BEC (e.g., [55]) is that it allows a convenient and natural integration between the steady-state prediction and calculation of dynamic evolution in interferometric scenarios.

B. Free expansion and collimation

The solution of Eq. (18) for a Gaussian wave packet in free space ($Q_j = 0$ and $a_s N \to 0$) is

$$\sigma_j(t) = \sigma_j(0)\sqrt{1 + \left(\frac{\hbar t}{2m\sigma_j(0)^2}\right)^2}, \tag{33}$$

where t is the time elapsed since the wave packet was at its minimum size $\sigma_j(0)$. This solution also applies to a Hermite-Gaussian wave packet of the form of Eq. (24) with σ_j being the width of the Gaussian. It follows that the law of expansion in Eq. (33) also holds for a thermal cloud that is initially a mixed state of Hermite-Gaussian states of a harmonic trap with $\hbar/2m\sigma_j(0)^2 = \omega_j$. The actual size $\sigma_{Tj} \equiv [\int d^3\mathbf{r}\, r_j^2 \rho(\mathbf{r})]^{1/2}$ in a given direction $\hat{r}_j$ of a thermal cloud of temperature T in a trap or after expansion is related to the Gaussian size of the wave packets as

$$\sigma_{Tj} = \sqrt{2n_{Tj} + 1}\sigma_j, \tag{34}$$

where n_{Tj} is the thermal occupation of the harmonic oscillator levels, approximated by $n_{Tj} \approx \frac{k_B T}{\hbar\omega_j}$ in the Boltzmann limit of high temperature $k_B T \gg \hbar\omega_j$. After a long time of expansion $\omega_j t \gg 1$ we reach the classical limit where $\sigma_{Tj}(t) \approx \sqrt{k_B T/m}t$ where the cloud is isotropic and its size is independent of the trap frequencies.

In the case of a cylindrically symmetric BEC for which $\sigma_y = \sigma_z = \sigma_\perp \gg \omega_x$ the first two terms on the right-hand side of Eq. (18) scale like $\sigma_\perp^{-3}$ and σ_x varies fairly slowly. Then over a timescale where $\sigma_x \equiv \sigma_\parallel$ is almost constant the solution for $\sigma_\perp$ has the same form as Eq. (33), with $\hbar^2/4m^2\sigma_j(0)^4$ multiplied by $1 + \beta a_s N/\sigma_\parallel$. The same expansion law holds for a cloud of noninteracting atoms or a BEC initially in an elongated trap,

$$\sigma_j(t) = \sigma_j(0)\sqrt{1 + \omega_j^2 t^2} \tag{35}$$

when the atoms are released abruptly from the trap at $t = 0$. This generalizes the TDTF result [36] obtained for a BEC in the TF regime. Note that Eq. (35) with $\sigma_j(0)$ and ω_j as arbitrary parameters can serve as a general solution of Eq. (18) in free space for any given initial conditions $\sigma_j(t_a)$, $\dot{\sigma}_j(t_a)$ at an arbitrary time t_a, in the case of no interactions or the transverse directions of an elongated BEC. This law of expansion (or focusing, if $t < 0$) is therefore useful in many cases beyond the case of abrupt release from a trap, as demonstrated below.

A common practice in matter-wave interferometers is the so-called "delta-kick collimation" [11,57], in which after trap release and some time T_e of expansion a pulse of duration T_c of harmonic potential (frequency ω_c) is applied in a specific direction $\hat{z}$ (or more than one direction). After this pulse the expansion is stopped and the cloud size is steady, as if it was released from a shallow trap holding a wide cloud. In the limit of a strong and short pulse the collimation imprints a phase $\phi(z) = -\frac{m}{2\hbar}\omega_c^2 T_c z^2$ that is designed to cancel the quadratic phase $\frac{1}{2}\alpha_z z^2$ due to expansion. If the expansion along x obeys Eq. (35), then $\alpha_z = (m/\hbar)\omega_0^2 T_e/(1 + \omega_0^2 T_e^2)$, where ω_0 is the initial trap frequency along $\hat{z}$. The pulse duration required for collimation should satisfy $\omega_c^2 T_c = \omega_0^2 T_e/(1 + \omega_0^2 T_e^2) \sim 1/T_e$. In Appendix A we calculate the exact required collimation pulse duration in the more general case of a nonabrupt pulse by using energy conservation during free expansion and during the collimation pulse. We show that the general solution of Eq. (18) in the above scenario where the repulsive term can be written as $\omega_0^2\sigma_0^4/\sigma_z^3$ is given by

$$\sigma_z(t) = \sigma_{\min}\sqrt{1 + \left[\left(\frac{\omega_0\sigma_0^2}{\omega_c\sigma_{\min}^2}\right)^2 - 1\right]\sin^2\omega_c t}, \tag{36}$$

where $\sigma_{\min}$ is determined by the initial conditions just before the harmonic pulse.

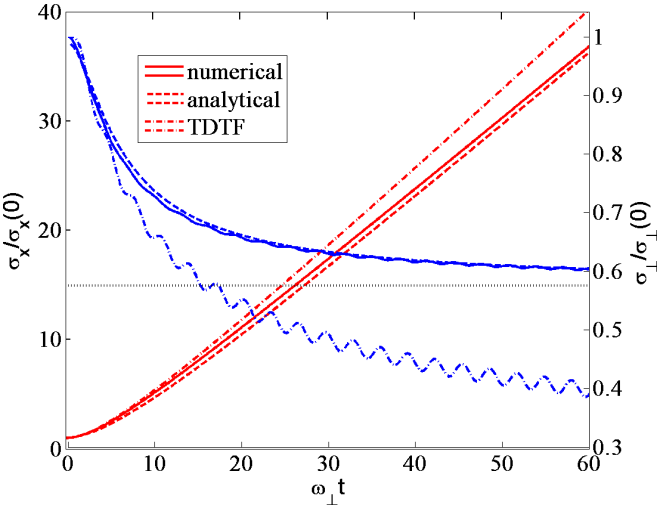

FIG. 3. BEC expansion in a waveguide. Comparison of a numerical (solid curves) and an analytical (dashed) solution of the unified wave-packet model for the longitudinal size (red curves, left axis) and transverse size (blue curves, right axis) of a BEC expanding in a waveguide. The numerical and analytical solutions for the transverse size are almost indistinguishable, but both are qualitatively different from the TDTF solution (dashed-dotted curves), which shrinks to much less than the single-particle transverse ground-state size $\ell_\perp = \sqrt{\hbar/2m\omega_\perp}$ (dotted line). The model assumes a BEC of 10^4 atoms in a waveguide potential with $\omega_\perp = 2\pi \times 100$ Hz and initial trap parameters as in Fig. 1. The analytical approximation for the longitudinal size $\lambda_x = \sigma_x/\sigma_x(0)$ uses Eq. (B9) with $n = 1$ (for simplicity the accuracy can be improved significantly by using $n = 1.1$). The analytical expression for the transverse size uses Eq. (B4) with σ_x given by the analytical approximation and $\beta = \beta_{3D}$ for simplicity.

C. BEC expansion in a waveguide

The unified wave-packet model is particularly essential in the field of guided interferometry with a BEC, where a BEC that is initially describable within the TF approximation expands in a waveguide. The expansion leads to a dynamical transition from the 3D BEC into a quasi-1D geometry where the atoms occupy dominantly the lowest energy transverse mode of the waveguide. In Fig. 3 we present the dynamics of the longitudinal and transverse sizes of the expanding BEC that was calculated with the unified model (solid curves) compared to an analytical approximation (dashed) derived in Appendix B and numerical results of the TDTF (dashed-dotted). When the longitudinal size of the expanding BEC σ_x is of the same order as $\beta a_s N$ (about 20 μm or six times

the initial longitudinal size in this example) the transverse kinetic force becomes dominant compared to the interaction force, while the latter is too weak to hold the BEC against the harmonic confinement potential. In this regime the TDTF fails to describe the correct dynamics, while the unified model can reproduce the correct behavior where the transverse size relaxes into the size of the lowest energy transverse mode. This calculation has a particularly important implication on the rate of phase diffusion when the BEC is split into a superposition of counter propagating wave packets inside the guide, as the rate of decoherence crucially depends on the atomic density.

D. Quick splitting into two traps

In the following example we examine the role of the atomic fraction parameter η when a cloud of interacting atoms is split into two clouds, each with roughly a half of the initial atom number. The uncertainty of the atom fraction after coherent splitting has an important role in the loss of coherence of interacting atoms through phase diffusion, but this effect, in the context of our model, will be discussed elsewhere. Here we will examine other dynamical aspects of the change of fraction during splitting.

Consider an interferometer in which an initially trapped BEC is split into two parts that remain trapped, as in the Sagnac interferometer proposed in Ref. [29]. Immediately after the two wave packets separate, each of them contains only $N/2$ particles that no longer satisfy the stationary GPE, not only due to the motion of the trap centers, as analyzed in Ref. [29], but also due to the change of the atom number in each trap. If the trap frequencies do not change, then the cloud first shrinks due to the reduced repulsive mean-field force, initiating breathing-mode oscillations around equilibrium values $\sigma_j^{\rm eq}$ determined by the steady-state solution of Eq. (18) with $\eta = 1/2$. As shown in the analysis of BEC expansion in a waveguide (Appendix B), the transverse oscillation frequency is twice the trap frequency if $\sigma_\perp \gg \sigma_\parallel$. In a similar way we can show that the oscillation frequency in the longitudinal direction is a factor of $\sqrt{2}$ larger than the longitudinal trap frequency.

Right after the splitting the interaction chemical potential [Eq. (17)] decreases by a factor of 2 and hence the phase variation in Eq. (25) slows down, but the shrinking of the sizes and their oscillations tend to increase the phase variation and compensate for the reduction due to the drop of the particle number in each wave packet.

In Fig. 4 we show the wave-packet sizes and central phase $\varphi(t)$ over one period of the transverse trap frequency, just after an infinitely quick splitting, where $\eta \to 1/2$ at $t = 0$. For emphasizing the details, the phase φ is scaled by the phase of the original wave packet $\varphi_0(t) = -\mu_{\rm tot} t/\hbar$ if no splitting occurred. In the case of a large number of atoms, approaching the TF limit, the initial phase reduces to about a half of the original phase, but then, when the wave packet shrinks and oscillates, the phase grows to a higher percentage of the unsplit wave-packet phase. The calculation based on Eqs. (22) and (25) agrees to less than about 1% accuracy with the result of the GPE (dots) except at very short times (less than a tenth of a period), where the total phase is a small fraction of a radian. It follows that for long times relevant to interferometry

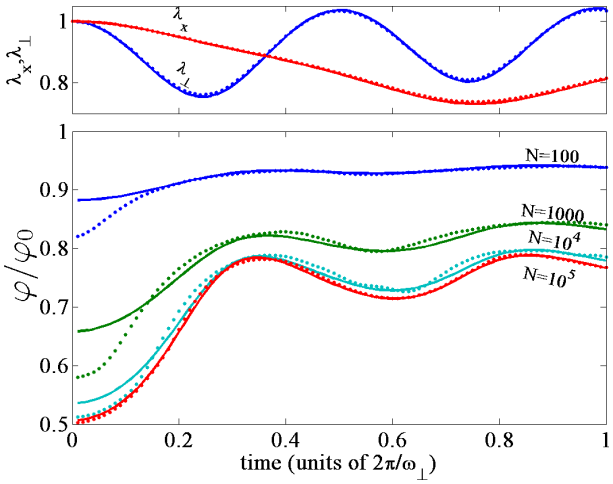

FIG. 4. Quick splitting into two separate traps: phase evolution after a sudden reduction of the atom number in each single trap to half the number before splitting—comparison between the unified wave-packet model (solid lines) and numerical GPE results (dots). Parameters before and after splitting are as in Fig. 1. The reduction of the repulsive mean-field potential by a factor $\eta = \frac{1}{2}$ causes breathing oscillations of the BEC (top panel, $N = 10^4$ atoms). The phase at the center of the wave packet $\varphi(t)$ (bottom panel) is shown scaled by the phase of the original wave packet $\varphi_0(t) = -\mu_{\rm tot} t/\hbar$ if it had not been split [$\mu_{\rm tot}$ is chemical potential given in Fig. 1(b)]. The wave-packet model agrees well with the numerical results except for a small number of atoms at short times (less than 1 ms) where the accumulated phase is much less than a radian.

the wave-packet model reproduces accurately the results of the exact numerical solution.

IV. SPATIAL COHERENCE

In this section we use the unified wave-packet model in the context of spatial coherence of interferometers with imperfect recombination of the two arms at the output port. We first present a general discussion of the concept of coherence length and then derive a more detailed theory of interferometric contrast upon imperfect recombination in both position and momentum. The unified wave-packet model enables predictions relevant to various interferometric configurations and various atomic sources, specifically a BEC with an arbitrary mean-field interaction strength.

A. Coherence length

Coherence length is a useful concept in interferometry. It is often considered as an intrinsic property of the quantum particles or waves used in the interferometer that depends on their preparation, but it can also evolve during the propagation, for example, due to coupling to the environment. The coherence length determines the contrast of the interferometric signal in the presence of path length differences between its arms but also determines the precision of interferometers designed to measure path length differences. Here we discuss the coherence of matter-wave interferometers designed to measure fields or forces by their effect on the relative phase between two paths that have virtually the same length. In this kind

of interferometers, which are used, for example, to measure acceleration or rotation, it is important that the recombination of the two arms at the output port is as accurate as possible. Path length differences larger than the coherence length lead to loss of contrast.

In an interferometer with a pure state input represented by a well-defined wave function that evolves through the interferometer arms as $\psi(\mathbf{r},t)$ a path length difference gives rise to a spatial displacement $\delta\mathbf{x}$ between the two arms at the output port that limits the contrast by the overlap integral

$$C(\delta\mathbf{x}) = \int d^3\mathbf{r}\,\psi^*(\mathbf{r}-\delta\mathbf{x}/2)\psi(\mathbf{r}+\delta\mathbf{x}/2), \tag{37}$$

where it is assumed that all the other features of the wave functions at the two arms are exactly the same except for the displacement $\delta\mathbf{x}$ and the phase accumulated along the arms. The coherence length $l_c(\hat{\boldsymbol{\xi}})$) for displacement along a specified direction $\delta\mathbf{x} = \delta x\hat{\boldsymbol{\xi}}$ is defined as half the distance of separation $|\delta x|2$ between the two wave-packet copies along the direction of the unit vector $\hat{\boldsymbol{\xi}}$ such that the contrast drops by $1/e^2$,

$$C(2l_c\hat{\boldsymbol{\xi}}) = 1/e^2. \tag{38}$$

By Fourier transforming the wave function $\psi(\mathbf{r})$ it is easy to see that the autocorrelation function can be written as

$$C(\delta\mathbf{x}) = \int d^3\mathbf{k}\,e^{i\mathbf{k}\cdot\delta\mathbf{x}}|\psi(\mathbf{k})|^2. \tag{39}$$

In general, the input of the interferometer is a mixed state described by a density matrix evolving in time like $\rho(\mathbf{r},\mathbf{r}',t) = \sum_n W_n\psi_n(\mathbf{r},t)\psi_n^*(\mathbf{r}',t)$, where ψ_n are a set of orthogonal wave functions and W_n are weights satisfying $\sum_n W_n = 1$. The overlap integral at the output of the interferometer becomes

$$C(\delta\mathbf{x}) = \sum_n W_n C_n(\delta\mathbf{x}) = \int d^3\mathbf{k}\,e^{i\mathbf{k}\cdot\delta\mathbf{x}}\rho(\mathbf{k},t), \tag{40}$$

where $\rho(\mathbf{k}) = \sum_n W_n|\psi_n(\mathbf{k})|^2$ is the probability of finding the particle at the output momentum $\hbar\mathbf{k}$. Let us consider a displacement along a certain axis $\hat{z}$ and assume that the momentum probability distribution is approximately a Gaussian $\rho(k_z) \equiv \int dk_x \int dk_y\,\rho(\mathbf{k}) \propto e^{-k_z^2/2\Delta k_z^2}$. In this case the contrast for a displacement δz is $C(\delta z) = e^{-\Delta k_z^2\delta z^2/2}$ so that the coherence length along $\hat{z}$ is

$$l_c(\hat{z}) = \frac{1}{\Delta k_z} = \frac{\hbar}{\Delta p_z}, \tag{41}$$

inversely proportional to the momentum uncertainty Δp_z.

More generally imperfect recombination leading to reduction of the coherence may also be due to other distortions of the output wave packets coming from the two arms relative to each other, such as width and spatially dependent phase. However, the most common one is momentum mismatch at the output port. This kind of mismatch is usually negligible in common atom interferometers based on laser pulses, which provide very accurate momentum kicks. Momentum mismatch is important, for example, in Stern-Gerlach interferometers where the momentum kicks are tunable rather than quantized. In analogy to the coherence length for position mismatch we define a momentum coherence width w_c for momentum mismatch, which is approximated by

$$w_c(\hat{z}) \approx \frac{\hbar}{\Delta z}, \tag{42}$$

where Δz is the position uncertainty of the atoms along $\hat{z}$ at the output port.

Here we develop a general theory that takes into account both position and momentum mismatch, which is based on our method of wave-packet evolution presented in Sec. II. This theory will be relevant to noninteracting thermal atomic clouds as well as BEC clouds with any strength of atom-atom interaction, provided that the interactions during splitting and recombination can be absorbed into parameters of the theory.

B. The overlap integral

The state at the output port of an interferometer with coherent input is a coherent superposition

$$\psi(\mathbf{r}) = A\psi_a(\mathbf{r}) + B\psi_b(\mathbf{r}), \tag{43}$$

where ψ_a and ψ_b are the spatial wave functions at the output of arms a and b, respectively, including phases due to propagation through the arms, while A and B ($|A|^2 + |B|^2 = 1$) are the corresponding amplitudes. For simplicity we assume that $A = B = 1/\sqrt{2}$, so that the detection probability at the output port is

$$\mathcal{P}_{\text{out}} = \frac{1}{2}[1 + C\cos(\delta\varphi)], \tag{44}$$

where the contrast C and phase $\delta\varphi$ are, respectively, the absolute value and phase of the overlap integral

$$Ce^{-i\delta\varphi} = \int d^3\mathbf{r}\,\psi_a^*(\mathbf{r})\psi_b(\mathbf{r}). \tag{45}$$

The overlap integral in Eq. (45) is invariant under any unitary operation on both wave functions ψ_a and ψ_b, for example, when the same potential is applied to both arms before reaching the output port. Let $\hat{U}(t,t_0)$ be a unitary time-evolution operator, such that $\psi_{a,b}(\mathbf{r},t) = \hat{U}(t,t_0)\psi_{a,b}(\mathbf{r},t_0)$. It follows that

$$\begin{aligned}\psi_a^*(\mathbf{r},t)\psi_b(\mathbf{r},t) &= \psi_a^*(\mathbf{r},t_0)\hat{U}^\dagger\hat{U}\psi_b(\mathbf{r},t_0)\\ &= \psi_a^*(\mathbf{r},t_0)\psi_b(\mathbf{r},t_0),\end{aligned} \tag{46}$$

so that the contrast and phase of the interference signal are independent of the time of measurement or the time where the output beam splitter is operated, as long as no differential forces are applied on the two arms.

Let us now separate the center motion from the internal wave-packet dynamics by expressing ψ_a and ψ_b in the form of Eq. (3). We concentrate on the effect of center position displacement $\delta\mathbf{x} \equiv \mathbf{R}_a - \mathbf{R}_b$ and momentum mismatch $\delta\mathbf{P} = \mathbf{P}_a - \mathbf{P}_b$ between the two arms, while other degrees of freedom are taken to be the same. Under the assumptions of Sec. II we take the two wave packets to have the form of Eq. (7) with the same shape, size, and expansion rate. We set the origin of the integration coordinates to be at $\mathbf{R} = \frac{1}{2}(\mathbf{R}_a + \mathbf{R}_b)$, so that $\mathbf{R}_{a,b} = \mathbf{R} \pm \delta\mathbf{x}/2$ and $\mathbf{P}_{a,b} = \mathbf{P} \pm \delta\mathbf{P}/2$, and obtain

$$C = \int d^3\mathbf{r}\,e^{-i\delta\tilde{\mathbf{K}}\cdot\mathbf{r}}\tilde{\Phi}_{\boldsymbol{\sigma}}\left(\mathbf{r} - \frac{1}{2}\delta\mathbf{x}\right)\tilde{\Phi}_{\boldsymbol{\sigma}}\left(\mathbf{r} + \frac{1}{2}\delta\mathbf{x}\right), \tag{47}$$

where

$$\delta\tilde{K}_j = \delta P_j/\hbar - \alpha_j \delta x_j \tag{48}$$

is the interference wave vector, which is related to the periodicity of a spatial fringe pattern that appears in interferometers of the double-slit type. The wave function $\tilde{\Phi}_{\boldsymbol{\sigma}}(\mathbf{r}) = \chi(\frac{x}{\sigma_1}, \frac{y}{\sigma_2}, \frac{z}{\sigma_3})/\sqrt{\sigma_1\sigma_2\sigma_3}$ is a normalized real function in which the phase factors of $\Phi(\mathbf{r}, t)$ were takend out.

The interferometric phase is

$$\delta\varphi = \phi_a - \phi_b - \mathbf{P}\cdot\delta\mathbf{x}/\hbar, \tag{49}$$

with

$$\phi_{a,b} = \frac{1}{\hbar}S_{a,b} + \varphi_{a,b}. \tag{50}$$

The phase accumulated along each interferometer arm (a or b) includes the action along the trajectory and the internal wave-packet phase [Eq. (25)] due to kinetic and interaction energy relative to the wave-packet center. The last term in Eq. (49) is often called "the separation phase" due to the separation between the two end points of the trajectories [58]. Together with this term the interferometric phase is invariant under free evolution, as required by Eq. (46), since $\delta S(t+\tau) - \delta S(t) = (P_a^2 - P_b^2)\tau/2m = \mathbf{P}\cdot\delta\mathbf{v}\tau$ is exactly canceled by the change of the separation phase $-\mathbf{P}\cdot\delta\mathbf{x}$ over the time τ.

An expression for the contrast similar to Eq. (47) is already given in Ref. [49]. Another expression that is suitable for interferometers based on free space propagation is obtained by utilizing the conservation law of Eq. (46) with the unitary operator $\hat{U} = e^{i\hbar\hat{p}^2\tau/2m}$ that propagates the wave packets back to the time $t-\tau$ where they were at their minimal size (i.e., before expansion). We obtain the result of Schwinger, Scully, and Englert [51]

$$C = \int d^3\mathbf{r}\,\psi_0^*\left(\mathbf{r} - \frac{1}{2}\delta\tilde{\mathbf{x}}\right)\psi_0\left(\mathbf{r} + \frac{1}{2}\delta\tilde{\mathbf{x}}\right)e^{-i\delta\mathbf{P}\cdot\mathbf{r}/\hbar}, \tag{51}$$

where ψ_0 is the wave function before expansion and $\delta\tilde{\mathbf{x}} \equiv \delta\mathbf{x} - \delta\mathbf{P}\tau/m$ is the final separation projected to the time before expansion. This expression is particularly useful because it implies that the coherence length of freely expanding non-interacting matter waves is conserved during propagation and determined by the momentum uncertainty of the initial wave packet before expansion.

C. Coherence of weakly interacting atoms

A Gaussian approximation for the wave function envelope in Eq. (47) $\tilde{\Phi}(_{\boldsymbol{\sigma}}\mathbf{r}) \propto \exp[-\frac{1}{4}\sum_j r_j^2/\sigma_j^2]$ yields $C = \prod_{j=1}^3 C_j$, where

$$\begin{aligned} C_j &= \exp\left[-\frac{\delta x_j^2}{8\sigma_j^2} - \frac{1}{2}\sigma_j^2\delta\tilde{K}_j^2\right] \\ &= \exp\left(-\frac{\delta x_j^2\zeta_j^2}{8\sigma_j^2} - \frac{\sigma_j^2\delta P_j^2}{2\hbar^2} + \frac{\sigma_j^2\alpha_j}{\hbar}\delta P_j\delta x_j\right), \end{aligned} \tag{52}$$

where

$$\zeta_j^2 = 1 + \left(\frac{2m}{\hbar}\sigma_j\dot{\sigma}_j\right)^2. \tag{53}$$

For a Gaussian wave packet in free space it is easy to see from Eq. (33) that $\zeta_j(t) = \sigma_j(t)/\sigma_j(0)$. For a pure position mismatch ($\delta\mathbf{P} = 0$) the contrast drops like $C_j = \exp[-\delta x_j^2/8\sigma_j(0)^2]$, such that the coherence length [defined in Eq. (38)] is $l_c(\hat{\mathbf{r}}_j) = 2\sigma_j(0)$, as follows from Eq. (51). For a pure momentum mismatch ($\delta\mathbf{x} = 0$) at the time of measurement, the contrast depends on the expansion time t_e before measurement $C_j = \exp[-\frac{1}{2}\sigma_j t_e^2\delta P_j^2/\hbar^2] \propto \exp[-\delta P_j^2 t_e^2/8m^2\sigma_j(0)^2]$. This corresponds to a t_e-dependent momentum coherence width $w_c = \hbar/\sigma_j(t_e)$, while the coherence length l_c is independent of the expansion time in free expansion where the momentum uncertainty is constant. It follows from the conservation of the overlap integral and may be verified explicitly that in the case of free expansion the contrast in Eq. (52) can be written in a time-independent form

$$C_j = \exp\left[-\frac{\delta x_j(0)^2}{8\sigma_j(0)^2} - \frac{1}{2\hbar^2}\sigma_j(0)^2\delta P_j^2\right], \tag{54}$$

where $\delta x_j(0) = \delta x_j(t) - \frac{1}{m}\delta P_j t$ is the position mismatch projected back to the time ($t = 0$) where the wave packet has a minimal size $\sigma_j(0)$. While Eq. (54) repeats previous results concerning freely expanding Gaussian wave packets, it is equivalent to the more general form in Eq. (52), which is valid for any evolution history before measurement, once we use the projected free-expansion values of $\sigma_j(0)$ and t. These values can be derived from the instantaneous values of σ_j and $\dot{\sigma}_j$ at the time of measurement, regardless of the real evolution history:

$$\sigma_j(0) = \frac{\sigma_j(t)}{\sqrt{1 + (2m\sigma_j\dot{\sigma}_j/\hbar)^2}}, \quad t = \left(\frac{2m\sigma_j(0)}{\hbar}\right)^2\sigma_j(t)\dot{\sigma}_j. \tag{55}$$

The result of Eq. (52) or its simplified version Eq. (54) can be generalized beyond the minimal uncertainty wave-packet case by using the law of conservation of the overlap integral [Eq. (46)] Let us assume that the input of the interferometer is a mixed state represented by a density matrix

$$\rho(\mathbf{r}, \mathbf{r}') = \sum_{\mathbf{n}} W_{\mathbf{n}}\psi_{\mathbf{n}}(\mathbf{r})\psi_{\mathbf{n}}^*(\mathbf{r}'), \tag{56}$$

where $\psi_{\mathbf{n}}(\mathbf{r}, t)$ are a set of functions based on the Gaussian-Hermite functions of Eq. (24) with common sizes $\sigma_j(t)$ and center coordinates due to the common history of evolution through the interferometer. The contrast at the output port has the general form

$$C = \int d^3\mathbf{r}\, e^{-i\delta\tilde{\mathbf{K}}\cdot\mathbf{r}}\ \tilde{\rho}_{\boldsymbol{\sigma}}\left(\mathbf{r} - \frac{1}{2}\delta\mathbf{x}, \mathbf{r} + \frac{1}{2}\delta\mathbf{x}\right),$$

where

$$\tilde{\rho}_{\boldsymbol{\sigma}}(\mathbf{r}, \mathbf{r}') = \sum_{\mathbf{n}} W_{\mathbf{n}}\tilde{\Phi}_{\mathbf{n},\boldsymbol{\sigma}}(\mathbf{r})\tilde{\Phi}_{\mathbf{n},\boldsymbol{\sigma}}^*(\mathbf{r}') \tag{57}$$

is the density matrix in the frame moving with the atomic clouds in the two arms. The functions $\tilde{\Phi}_{\mathbf{n},\boldsymbol{\sigma}}$ are eigenstates of a harmonic Hamiltonian $\hat{H} = \sum_j \hat{H}_j$ with frequencies

$\nu_j = \hbar/2m\sigma_j^2$:

$$\hat{H}_j(\sigma_j) = \frac{\hat{p}_j^2}{2m} + \frac{1}{2}m\nu_j^2\hat{r}_j^2 = \hbar\nu_j\left[\left(\frac{\sigma_j\hat{p}_j}{\hbar}\right)^2 + \left(\frac{\hat{r}_j}{2\sigma_j}\right)^2\right]. \tag{58}$$

Hence, applying a unitary operator $\hat{U} = \exp[-i\sum_j \hat{H}_j t_j/\hbar]$ to these functions does not change the functions but only creates a rotation of their center position and momentum in phase space. The Hamiltonians (58) preserve the quadratic form $(\sigma_j p_j/\hbar)^2 + \frac{1}{4}(r_j/\sigma_j)^2$. By choosing appropriate parameters t_j we can therefore perform a unitary transformation equivalent to a phase space rotation

$$\pm\delta x_j \to 0, \quad \pm\delta\tilde{K}_j \to \pm\sqrt{\delta\tilde{K}_j^2 + \frac{1}{4}\delta x_j^2/\sigma_j^4}. \tag{59}$$

We therefore obtain as a consequence of the conservation of the overlap integral

$$C = \int d^3\mathbf{r}\, e^{-i\sum_j r_j\sqrt{\delta\tilde{K}_j^2 + \frac{1}{4}\delta x_j^2/\sigma_j^4}}\rho_{\boldsymbol{\sigma}}(\mathbf{r}), \tag{60}$$

where $\rho_{\boldsymbol{\sigma}}(\mathbf{r}) = \tilde{\rho}_{\boldsymbol{\sigma}}(\mathbf{r},\mathbf{r})$ is the normalized density of atoms in the frame moving with the atomic cloud in each arm at the time of measurement, while assuming that the density of the two clouds is the same except for position and momentum shifts.

Let us now assume that the atomic cloud density $\rho(\mathbf{r})$ of each of the arms at the output oprt of the interferometer can be approximated by a Gaussian of widths Δx_j:

$$\rho_{\boldsymbol{\sigma}}(\mathbf{r}) \propto \exp\left(-\frac{1}{2}\sum_j r_j^2/\Delta x_j^2]\right). \tag{61}$$

When this distribution is Fourier transformed to give the contrast in Eq. (40) we obtain

$$C_j \approx \exp\left[-\Delta x_j^2\left(\frac{\delta P_j^2}{2\hbar^2} + \frac{\delta x_j^2\zeta_j^2}{8\sigma_j^4} - \frac{\alpha_j}{\hbar}\delta P_j\delta x_j\right)\right], \tag{62}$$

where ζ_j is given in Eq. (53).

For a thermal cloud, where $\Delta x_j = \sigma_j\sqrt{2\langle n_j\rangle + 1}$ the coherence length is

$$l_c(\hat{\mathbf{x}}_j) = \frac{2\sigma_j}{\zeta_j\sqrt{2\langle n_j\rangle + 1}} = \frac{\hbar}{\Delta p_j}, \tag{63}$$

where $\langle n_j\rangle$ is the average occupation of the initial harmonic oscillator states and Δp_j is the momentum uncertainty in the direction $\hat{\mathbf{r}}_j$, given by

$$\Delta p_j = \frac{\sqrt{2\langle n_j\rangle + 1}\hbar}{2\sigma_j(0)}, \tag{64}$$

where $\sigma_j(0) = \sigma_j/\zeta_j$ is given explicitely in Eq. (55). In particular, an atomic gas in thermal equilibrium with a Boltzmann distribution in a harmonic trap of frequency ω_j ($k_BT \gg \hbar\omega_j$) has an occupation $\langle n_j\rangle_T \approx k_BT/\hbar\omega_j$ and position-momentum uncertainties $\Delta x_j = \sigma_j(0)\sqrt{2\langle n_j\rangle + 1} \approx \sqrt{k_BT/m\omega_j^2}$ and $\Delta p_j = \sqrt{2\langle n\rangle_T + 1}/2\sigma_j(0) = \sqrt{mk_BT}$. The coherence length is then

$$l_c(\hat{\mathbf{x}}_j) \approx \frac{\hbar}{\sqrt{mk_BT}} \tag{65}$$

and time-independent in free expansion. The momentum coherence width is simply given by

$$w_c(\hat{\mathbf{x}}_j) = \frac{\hbar}{\sigma_j(t_e)\sqrt{2\langle n_j\rangle_T + 1}} \approx \sqrt{\frac{m}{k_BT}}\frac{\hbar\omega_j}{\sqrt{1+\omega_j^2t_e^2}}, \tag{66}$$

where t_e is the expansion time before measurement. While this coherence width depends on the time of measurement, the contrast C can be shown to be independent of time when the time-dependent position mismatch $\delta\mathbf{x}$, which grows linearly with $\delta\mathbf{P}/m$, is taken into account.

The coherence with respect to position mismatch or momentum mismatch can be improved by using gradual release from the trap or δ-kick collimation as described in Sec. III B. The effect of both procedures is to decrease the rate of expansion as if the cloud was released from a trap with a lower harmonic frequency $\omega_j' \ll \omega_j$ with a larger projected minimal cloud size $\sigma_j^{(0)}$. In this process the mean occupation numbers of the harmonic oscillator levels $\langle n_j\rangle \approx k_BT/\hbar\omega_j$ do not change, while the effective frequency changes, so that the effective temperature decreases to $T \to T' = (\omega_j'/\omega_j)T$.In this sense the δ-kick process is also called "cooling." This leads to the decrease of the kinetic energy and hence to the increase of the coherence length, and at the same time it may lead to the increase of the momentum coherence width for times small enough such that $\omega_j t_e \ll 1$, with ω_j being the effective harmonic frequency of the beam projected to its minimal size.

D. Coherence length of a BEC

The expression in Eq. (52) for the contrast of an interferometer with pure state input is exact for Gaussian wave packets, but it may also serve as a good approximation for a non-Gaussian BEC once the wave-packet sizes σ_j at the time of measurement are calculated. For example, a 3D inverted parabolic wave function [TF limit; Eq. (47)] yields for a pure position displacement along the x axis $C(\delta x, \delta\tilde{\mathbf{K}} = 0) \approx \exp[-(\delta x/2\xi_{TF,x}\sigma_x)^2/2]$ with $\xi_{TF,x} = 0.8267$, while for a pure momentum displacement $C(\delta\mathbf{x} = 0, \delta P_x) \approx \exp[-(\xi_{TF,p}\sigma_x\delta P_x/\hbar)^2/2]$ with $\xi_{TF,p} = 1.08$. This dependence, which is obtained by numerical integration and Gaussian fit, is demonstrated in Fig. 5. Different results are obtained for an expanding BEC with $\dot{\sigma} \neq 0$, as shown below. For an accurate estimation with arbitrary displacements one must perform a direct numerical integration of Eq. (47).

For a freely expanding cylindrical BEC the expansion in the transverse direction after turning off the trap is given by Eq. (35) and hence $\zeta_\perp(t) = \sqrt{1+\omega_\perp^4t^2/\nu_\perp^2}$, where $\nu_\perp^2 = \hbar/2m\sigma_{\rm perp}(0)^2$. The coherence length $l_c(\hat{\mathbf{x}}_\perp) = 2\sigma_\perp(t_e)/\zeta_\perp(t_e)$ becomes

$$l_c(\hat{\mathbf{x}}_\perp) = 2\sigma_\perp(0)\sqrt{\frac{1+\omega_\perp^2t^2}{1+[\sigma_\perp(0)/\ell_\perp]^4\omega_\perp^2t^2}}, \tag{67}$$

where $\ell_\perp$ is the transverse harmonic oscillator length, as defined in Eq. (26). The coherence length of a BEC is initially equal to the half width of the cloud size at $1/e^2$ of the maximum, and then after expansion it drops by a factor of $[\ell_\perp/\sigma_\perp(0)]^2$ (at $t \gg \omega_\perp^{-1}$ and becomes smaller than the cloud

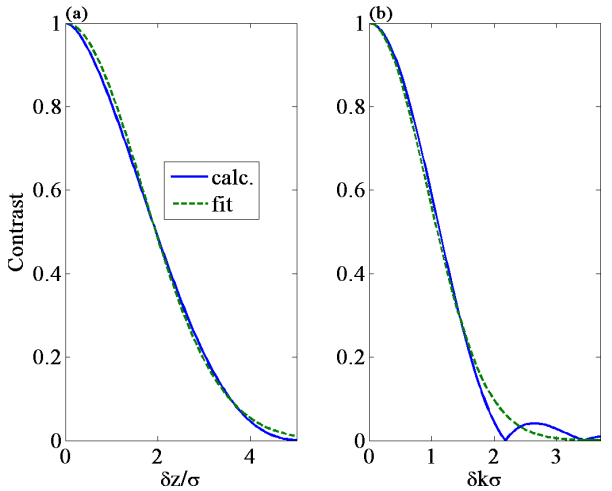

FIG. 5. Contrast drop due to position displacement (a) or momentum displacement (b) of a BEC in the TF limit before expansion, having an inverted parabolic density and flat phase. The solid curves are obtained by a numerical integration, while the dashed curves are Gaussian fits, resulting in $\xi_{TF,x} = 0.8267$ and $\xi_{TF,p} = 1.08$ (see text).

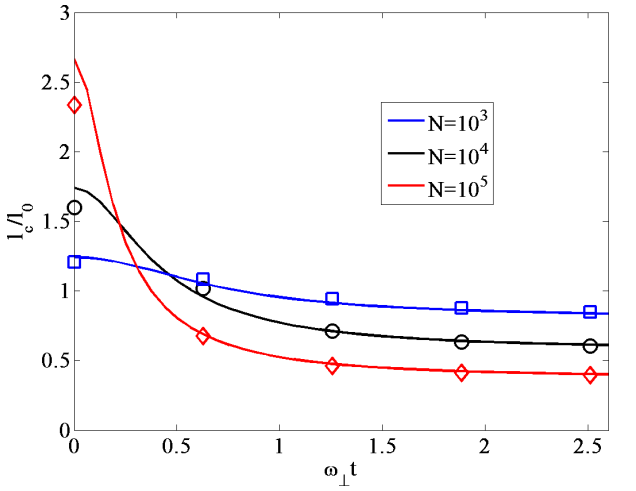

FIG. 6. Transverse coherence length $l_c(\hat{\mathbf{x}}_\perp)$ of a BEC as a function of free expansion time in units of the coherence length of noninteracting atoms $l_0 = 2\ell_\perp$. The coherence length is defined as half the length δx to which the wave packets of the two interferometer arms at the output port are separated along the transverse direction such that the interference contrast drops to $1/e^2$ [Eq. (38)]. It is extracted from the fit of the contrast in Eq. (37) to a Gaussian $C(\delta x) = \exp[-(\delta x/l_c)^2/2]$, where the wave packet $\psi(\mathbf{r})$ is obtained from a numerical solution of the GPE (symbols). The solid lines represent the approximation (67) with the value of $\sigma_\perp(0)$ calculated from Eq. (27). Trap and BEC parameters are as in Fig. 1. Good agreement between the predictions of the model and exact numerical results is obtained for all interaction strength regimes. The discrepancies at short times may be attributed to the non-Gaussian shape of the BEC, as discussed in Fig. 5.

size $2\ell_\perp$ of a single atom in the trap,

$$l_c(\hat{\mathbf{x}}_\perp, t \gg \omega_\perp^{-1}) = 2\ell_\perp \frac{\ell_\perp}{\sigma_\perp(0)}. \tag{68}$$

This reduction of the coherence may be attributed to the increase of momentum uncertainty when the interaction energy turns into kinetic energy during expansion.

In Fig. 6 we show the coherence length of a BEC as a function of expansion time for a typical trap $[(\omega_\parallel, \omega_\perp) = 2\pi \times (40, 100)$ Hz] with different atom numbers N: weak interactions ($N = 10^3$), moderate interactions ($N = 10^4$), and strong interactions ($N = 10^5$). The coherence length is in units of the coherence length l_0 of noninteracting atoms $l_0 = 2\ell_\perp$. For interacting atoms the initial coherence length is larger than l_0, and then it drops to values that are lower than l_c. The analytical approximation in Eq. (67) agrees fairly well with the numerical calculation based on a full solution of the GPE. The relatively small discrepancies may be attributed to the non-Gaussian shape of the BEC, as discussed above around Fig. 5.

Note that a collimation procedure as discussed in Sec. III B and in Sec. IV C in the context of a thermal cloud can be used to increase the coherence length of a BEC as well. In this case one should replace $\sigma_\perp(0)$ and $\omega_\perp$ in Eqs. (67) and (68) with the values corresponding to the wave-packet size after collimation and the effective harmonic frequency $\omega_\perp \sim \hbar/2m\sigma_\perp(0)^2$ if the collimation process ends with an atomic density where the interactions become negligible. Otherwise, if interactions are important over the whole process, such as in the case of a guided interferometer with a BEC, one should calculate the evolution of the BEC sizes σ_j over the interferometer arms and then use Eq. (52) as a Gaussian approximation for the overlap integral, so that $l_c = 2\sigma_j(t)/\zeta_j(t)$ at the time of measurement.

V. CONCLUSIONS AND OUTLOOK

The unified wave-packet evolution theory presented here provides an efficient tool for calculating the performance of atomic interferometers based on trapped, guided, or freely propagating atomic clouds. It is valid for atomic evolution in a variety of static or time-dependent potentials for trapping, guiding, or accelerating matter waves and for atom-atom interactions ranging from negligible interactions (as for a single atom or a dilute thermal cloud) to a strongly interacting BEC, as long as the condensate approximation holds. This model generalizes previous approaches that were valid for certain ranges of interactions or potentials [37,44,49]. We demonstrate the model with simple examples: a stationary BEC in a cylindrical trap with a relatively low aspect ratio between the trap axes or a very high aspect ratio with a transition between a 3D and a quasi-1D BEC and dynamical evolution when a trapped BEC is released into free space or a waveguide, collimated, or split into two separate traps (Sec. III). While our model coincides with well-established approximations and is hence guaranteed to be valid in the weak and strong limits of atom-atom interactions, we establish its validity in the intermediate regime by comparing some of the numerical and analytical calculations based on the unified model with direct solutions of the GPE and obtain excellent agreement over the whole range of atomic interactions.

For the situations discussed in this work, we stress that wave-packet dynamics could, in principle, be calculated by direct numerical solution of the Schrödinger equation or the GPE. However, in many practical cases that involve propagation over long times and/or distances, a precise numerical calculation is very difficult or impossible, especially if many calculations are necessary in order to design, analyze, or optimize the performance of the system under various conditions. The present work offers an efficient tool that can cope with such tasks and provide reliable results. In addition, this work includes numerous analytical results that provide insight and understanding of the underlying physics, which would not be apparent from complex numerical calculations. Furthermore, the numerical procedure needed to solve this model is very simple and does not require expertise in numerics. Beyond the solution of Newton's equations for the center coordinates of the wave packet, it involves the solution of ordinary differential equations for six parameters: the wave-packet sizes along the three cartesian directions and their time derivatives [Eq. (18)]. This set of parameters provides all the necessary information for predicting interferometric performance in various scenarios.

The theory of spatial coherence in Sec. IV generalizes the theory of spin coherence of a Stern-Gerlach interferometer [50–52] and the more recent theory of contrast in modern atomic interferometers [49] to include the whole range of atom-atom interactions. In particular, we analyze the contrast of atomic interferometers in terms of coherence length and show how the coherence length of a BEC changes during free expansion due to the increase of momentum uncertainty. Our theory provides an analytical prediction that reproduces the coherence length of an expanding BEC, to a good precision over the whole range of atom-atom interactions, a prediction that was not completely successful in a previous work [44].

One novelty of this work that makes it most suitable for treating various interferometric scenarios is that it includes effects due to changing the number of atoms in a BEC wave packet when an initial cloud is split into separate clouds, each including a fraction of the total number of atoms. One of the important consequences of the dependence of the evolution on atom number is phase diffusion due to atom-atom interactions, which arises from the number uncertainty after splitting. The discussion of phase diffusion in time-dependent interferometric scenarios is expected to benefit greatly from our model and will be discussed elsewhere.

The utility of the method presented in this work has already been demonstrated in the analysis and optimization of the phase stability of a spatial fringe Stern-Gerlach interferometer [45], as discussed briefly in the introduction. The simple examples examined in Secs. III C and III D provide insight into possible analyses of recent experimental results or proposals involving interferometry in waveguides [48] or moving traps [29], although a thorough analysis of these particular experiments with the unified model is beyond the scope of this paper.

Finally, let us mention three possible extensions of the wave-packet evolution theory, beyond the scope of this paper, that would make it more general and effective. First, the current theory is based on the assumption that a quadratic expansion of the external potential around the wave-packet center is sufficient to describe the evolution. One would like to define quantitatively the range of validity of this assumption and examine the negligible possible effects of higher-order terms of the potential. Second, we have not considered rotational effects when the axes of the time-dependent external potential do not coincide with the axes of the initial trap. This case could possibly be treated in a way similar to what was presented in Ref. [37], and one would expect a synthesis of that method with the present work. Third, we have not provided an explicit form for the wave-packet envelope, which was assumed to be an implicit interpolation between a Gaussian and an inverted parabola. A more explicit approximation for the envelope in the initial trap and its evolution could possibly be worked out as an extension of the present work and provide more details regarding properties of the wave packet that were not discussed here.

ACKNOWLEDGMENTS

I am grateful to the members of the BGU atom chip group for useful discussions and helpful comments, particularly to M. Keil, Y. Margalit, D. Groswasser, S. Moukouri, and R. Folman. I also acknowledge support from the Israeli Council for Higher Education. This work is funded in part by the Israel Science Foundation, Grant No. 856/18 and by the German-Israeli Foundation for Scientific Research and Development, Hybrid devices: FO 703/2-1.

APPENDIX A: DETAILED COLLIMATION PROCESS

Consider a noninteracting atom cloud or an elongated cylindrically symmetric BEC over a time duration where the expansion along the longitudinal axis is negligible. Let us define σ_0 as the wave-packet width along the relevant axis at the time of trap release, σ_e after free expansion and σ_f after the collimation pulse. During the collimation pulse of frequency ω_c the equation of motion for σ in the relevant direction is

$$\ddot{\sigma} = \frac{\omega_0^2\sigma_0^4}{\sigma^3} - \omega_c^2\sigma, \tag{A1}$$

where the first term on the right-hand side is consistent with the fact that in the original trap, where the size of the wave packet is σ_0, the wave packet is in steady state. This equation of motion corresponds to a conserved energy

$$E = \frac{1}{2}m\left(\dot{\sigma}^2 + \frac{\omega_0^2\sigma_0^4}{\sigma^2} + \omega_c^2\sigma^2\right). \tag{A2}$$

The solution of the equation of motion is given by

$$\sigma(t) = \sigma_{\min}\sqrt{1 + \left[\frac{\omega_0^2}{\omega_c^2}\left(\frac{\sigma_0}{\sigma_{\min}}\right)^4 - 1\right]\sin^2(\omega_c(t-t_0)}, \tag{A3}$$

where the minimal size $\sigma_{\min}$ and the time t_0 are determined by initial conditions. In the free space limit $\omega_c \to 0$ we have $\sigma_{\min} = \sigma_0$, and the expression reduces to the simple free-space solution $\sigma(t) = \sigma_0\sqrt{1+\omega_0^2t^2}$. For a finite ω_c the solution can also be written as

$$\sigma(t) = \sigma_{\max}\sqrt{1 - \left(1 - \frac{\sigma_{\min}^2}{\sigma_{\max}^2}\right)\cos^2\omega_c(t-t_0)}, \tag{A4}$$

where $\sigma_{\max} = \omega_0\sigma_0^2/\omega_c\sigma_{\min}$. In order to find the required duration T_c of the collimation pulse we need to find the final wave-packet size $\sigma_f = \sigma_{\max}$ and then calculate the time for which $\sigma(t) = \sigma_e$, where σ_e is the size of the wave packet at the beginning of the pulse. We then find

$$T_c = \frac{1}{\omega_c}\sqrt{\operatorname{asin}\left(1 - \frac{\sigma_e^2}{\sigma_f^2}\right)}. \tag{A5}$$

Let us now find the final size σ_f. From conservation of energy during the expansion time of duration T_e we deduce that the energy just before the beginning of the collimation pulse is equal to the initial energy just after trap release $E(t < T_e) = \frac{1}{2}m\omega_0^2\sigma_0^2$. The energy during the collimation pulse is then the energy before it plus the harmonic potential energy, so that

$$E(t > T_e) = \frac{1}{2}m\left(\omega_0^2\sigma_0^2 + \omega_c^2\sigma_e^2\right). \tag{A6}$$

In the end of the collimation pulse we wish to reach the maximal value of σ, where $\dot{\sigma} = 0$. Both $\sigma_{\min}$ and $\sigma_f = \sigma_{\max}$ are found by solving the quadratic equation for the conservation of energy during the collimation pulse

$$\omega_0^2\sigma_0^2 + \omega_c^2\sigma_e^2 = \omega_0^2\sigma_0^4/\sigma^2 + \omega_c^2\sigma^2. \tag{A7}$$

This has the solutions

$$\begin{aligned}\frac{\sigma_\pm^2}{\sigma_e^2} &= \frac{1}{2}(1+\xi^)\pm\frac{1}{2}\sqrt{(1+\xi^2)^2 - 4\xi^2/M_e^2}\\ &\approx 1 + \xi^2\left(1 - M_e^{-2}\right),\end{aligned} \tag{A8}$$

where $\xi = \omega_0\sigma_0/\omega_c\sigma_e$ and $M_e = \sigma_e/\sigma_0 = \sqrt{1+\omega_0^2T_e^2}$ is the "magnification" factor during expansion. The final wave-packet size $\sigma_f \equiv \sigma_+$ can now be substituted in Eq. (A5), such that if $\xi \ll 1$ we have

$$T_c \approx \frac{\xi\sqrt{1-M_e^{-2}}}{\omega_c} = \frac{\omega_0^2T_e}{\omega_c^2\left(1+\omega 0^2T_e^2\right)} \approx \frac{1}{\omega_c^2T_e}, \tag{A9}$$

where the last expression is valid when $\omega_0T_e \gg 1$.

APPENDIX B: ANALYTICAL SOLUTION FOR BEC EXPANSION IN A WAVEGUIDE

Let us consider the expansion of a BEC inside a waveguide with transverse frequency $\omega_\perp$. The coupled equations of motion can be written as

$$\ddot{\sigma}_x = \frac{\omega_\perp^2\ell_\perp^4\beta a_sN}{\sigma_\perp^2\sigma_x^2}, \tag{B1}$$

$$\ddot{\sigma}_\perp = \frac{\omega_\perp^2\ell\_\perp^4}{\sigma_\perp^3}\left(1+\beta\frac{a_sN}{\sigma_x}\right) - \omega_\perp^2\sigma_\perp, \tag{B2}$$

where $\ell_\perp = \sqrt{\hbar/2m\omega_\perp}$ and we have neglected the position-momentum uncertainty term in the equation for the longitudinal size. If we assume that initially $\sigma_x \gg \sigma_\perp$ and that the initial transverse frequency of the trap is not much different from the transverse frequency of the guide, then we expect the dynamics of the BEC to be characterized by oscillations of the transverse size $\sigma_\perp$ on a timescale of the order of the period of the transverse trap, while the expansion dynamics in the longitudinal direction has a much longer timescale. Let us therefore first examine the transverse dynamics while σ_x is steady ("Born approximation"). The corresponding potential for a given value of σ_x is

$$V_\perp(\sigma_\perp) = \frac{1}{2}m\omega_\perp^2\left[\frac{\ell_\perp^4}{\sigma_\perp^2}(1+\beta a_sN/\sigma_x) + \sigma_\perp^2\right]. \tag{B3}$$

This potential has a minimum at

$$\sigma_\perp^{\rm eq} = \ell_\perp\left(1+\frac{\beta a_sN}{\sigma_x}\right)^{1/4}. \tag{B4}$$

This value at the minimum of the potential is the equilibrium point for the oscillations of $\sigma_\perp$, whose frequency is obtained from the curvature of the transverse potential at the equilibrium size, and can be easily shown to be

$$\omega_{\rm osc} = \sqrt{V_\perp''(\sigma_\perp^{\rm eq})/m} = 2\omega_\perp. \tag{B5}$$

Next, we go on to the equation for the longitudinal size and replace $\sigma_\perp$ by its average over the timescale of change of the longitudinal dynamics, which is assumed to be the equilibrium value. We then obtain the equation

$$\ddot{\sigma}_x = \frac{\hbar\omega_\perp}{2m\sigma_x^2}\frac{\beta a_sN}{\sqrt{1+\beta a_sN/\sigma_x}}. \tag{B6}$$

This equation is equivalent to the evolution of a particle in a potential given by the integral of the right-hand side, namely,

$$V_x(\sigma_x) = \hbar\omega_\perp\sqrt{1+\beta a_sN/\sigma_x}. \tag{B7}$$

From conservation of energy it follows that

$$\begin{aligned}\frac{1}{2}m\dot{\sigma}_x^2 &= \hbar\omega_\perp\left[\sqrt{1+\frac{\beta a_sN}{\sigma_x(0)}} - \sqrt{1+\frac{\beta a_sN}{\sigma_x(t)}}\right]\\ &= 2m\omega_\perp^2[\sigma_\perp^{\rm eq}(0)^2 - \sigma_\perp^{\rm eq}(t)^2].\end{aligned} \tag{B8}$$

Note that at long times, such that $\sigma_x \gg \beta a_sN$, the rate of change of σ_x becomes constant $\dot{\sigma}_x \to 2\omega_\perp\sqrt{\sigma_\perp^{\rm eq}(0)^2 - \ell_\perp^2}$. At very short times we have $\sigma_x(t) \sim \sigma_x(0)[1+at^2]$, where $a = \frac{1}{2}\omega_\perp^2\ell_\perp^4\beta a_sN/\sigma_x(0)^3(\sigma_\perp^{\rm eq})^2$. In order to approximate the solution while satisfying the requirements in both limits we propose the form

$$\sigma_x(t) = \sigma_x(0)\left(1+\frac{at^2}{[1+(bt)^n]^{1/n}}\right), \tag{B9}$$

where $b = \sigma_x(0)a/\dot{\sigma}_x(\infty)$ and n is a free parameter that can be adjusted by a more complex investigation. In the demonstration of Fig. 3 we chose $n = 1$ for simplicity but find that $n = 1.1$ can provide a much better approximation for the numerical result.

[1] A. D. Cronin, J. Schmiedmayer, and D. E. Pritchard, Rev. Mod. Phys. **81**, 1051 (2009).

[2] J.-F. Schaff, T. Langen, and J. Schmiedmayer, in *Atom Interferometry*, edited by G. M. Tino and M. A. Kasevich, Proceedings of the International School of Physics "Enrico Fermi" Vol. 188 (IOS Press, 2014), pp. 1–87.

[3] C. Bordé, Phys. Lett. A **140**, 1 (1989).

[4] M. Kasevich and S. Chu, Phys. Rev. Lett. **67**, 181 (1991).

[5] T. L. Gustavson, P. Bouyer, and M. A. Kasevich, Phys. Rev. Lett. **78**, 2046 (1997).

[6] B. Canuel, F. Leduc, D. Holleville, A. Gauguet, J. Fils, A. Virdis, A. Clairon, N. Dimarcq, C. J. Bordé, A. Landragin, and P. Bouyer, Phys. Rev. Lett. **97**, 010402 (2006).

[7] X. Wu, F. Zi, J. Dudley, R. J. Bilotta, P. Canoza, and H. R. Müller, Optica **4**, 1545 (2017)

[8] Y.-J. Wang, D. Z. Anderson, V. M. Bright, E. A. Cornell, Q. Diot, T. Kishimoto, M. Prentiss, R. A. Saravanan, S. R. Segal, and S. Wu, Phys. Rev. Lett. **94**, 090405 (2005).

[9] O. Garcia, B. Deissler, K. J. Hughes, J. M. Reeves, and C. A. Sackett, Phys. Rev. A **74**, 031601(R) (2006).

[10] J. H. T. Burke, B. Deissler, K. J. Hughes, and C. A. Sackett, Phys. Rev. A **78**, 023619 (2008).

[11] H. Müntinga, H. Ahlers, M. Krutzik, A. Wenzlawski, S. Arnold, D. Becker, K. Bongs, H. Dittus, H. Duncker, N. Gaaloul *et al.*, Phys. Rev. Lett. **110**, 093602 (2013).

[12] B. Plotkin-Swing, D. Gochnauer, K. E. McAlpine, E. S. Cooper, A. O. Jamison, and S. Gupta, Phys. Rev. Lett. **121**, 133201 (2018).

[13] Y. Shin, M. Saba, T. A. Pasquini, W. Ketterle, D. E. Pritchard, and A. E. Leanhardt, Phys. Rev. Lett. **92**, 050405 (2004).

[14] L. A. Collins, L. Pezzé, A. Smerzi, G. P. Berman, and A. R. Bishop, Phys. Rev. A **71**, 033628 (2005).

[15] T. Schumm, S. Hofferberth, L. M. Andersson, S. Wildermuth, S. Groth, I. Bar-Joseph, J. Schmiedmayer, and P. Krüger, Nat. Phys. **1**, 57 (2005).

[16] G.-B. Jo, Y. Shin, S. Will, T. A. Pasquini, M. Saba, W. Ketterle, D. E. Pritchard, M. Vengalattore, and M. Prentiss, Phys. Rev. Lett. **98**, 030407 (2007).

[17] S. Machluf, Y. Japha, and R. Folman, Nat. Commun. **4**, 2424 (2013).

[18] Y. Margalit, Z. Zhou, S. Machluf, D. Rohrlich, Y. Japha, and R. Folman, Science **349**, 1205 (2015).

[19] O. Amit, Y. Margalit, O. Dobkowski, Z. Zhou, Y. Japha, M. Zimmermann, M. A. Efremov, F. A. Narducci, E. M. Rasel, W. P. Schleich, and R. Folman, Phys. Rev. Lett. **123**, 083601 (2019).

[20] S. Gupta, K. W. Murch, K. L. Moore, T. P. Purdy, and D. M. Stamper-Kurn, Phys. Rev. Lett. **95**, 143201 (2005).

[21] S. Wu, E. Su, and M. Prentiss, Phys. Rev. Lett. **99**, 173201 (2007).

[22] Y. Japha, O. Arzouan, Y. Avishai, and R. Folman, Phys. Rev. Lett. **99**, 060402 (2007).

[23] P. M. Baker, J. A. Stickney, M. B. Squires, J. A. Scoville, E. J. Carlson, W. R. Buchwald, and S. M. Miller, Phys. Rev. A **80**, 063615 (2009).

[24] B. E. Sherlock, M. Gildemeister, E. Owen, E. Nugent, and C. J. Foot, Phys. Rev. A **83**, 043408 (2011).

[25] A. Turpin, J. Polo, Yu. V. Loiko, J. Kuber, F. Schmaltz, T. K. Kalkandjiev, V. Ahufinger, G. Birkl, and J. Mompart, Opt. Express **23**, 1638 (2015).

[26] P. Navez, S. Pandey, H. Mas, K. Poulios, T. Fernholz, and W. von Klitzing, New J. Phys. **18**, 075014 (2016).

[27] S. Pandey, H. Mas, G. Drougakis, P. Thekkeppatt, V. Bolpasi, G. Vasilakis, K. Poulios and W. von Klitzing, Nature (London) **570**, 205 (2019).

[28] K. S. Hardman, C. C. N. Kuhn, G. D. McDonald, J. E. Debs, S. Bennetts, J. D. Close, and N. P. Robins, Phys. Rev. A **89**, 023626 (2014)

[29] R. Stevenson, M. R. Hush, T. Bishop, I. Lesanovsky, and T. Fernholz, Phys. Rev. Lett. **115**, 163001 (2015).

[30] E. R. Moan, R. A. Horne, T. Arpornthip, Z. Luo, A. J. Fallon, S. J. Berl, and C. A. Sackett, Phys. Rev. Lett. **124**, 120403 (2020)

[31] M. Lewenstein and L. You, Phys. Rev. Lett. **77**, 3489 (1996).

[32] J. Javanainen and M. Wilkens, Phys. Rev. Lett. **78**, 4675 (1997); A. J. Leggett and F. Sols, *ibid.* **81**, 1344 (1998); J. Javanainen and M. Wilkens, *ibid.* **81**, 1345 (1998).

[33] Y. Castin and J. Dalibard, Phys. Rev. A **55**, 4330 (1997).

[34] F. Dalfovo, S. Giorgini, and L. P. Pitaevskii, Rev. Mod. Phys. **71**, 463 (1999)

[35] J.-F. Mennemann, D. Matthes, R.-M. Weishäupl, and T. Langen, New J. Phys. **17**, 113027 (2015).

[36] Y. Castin and R. Dum, Phys. Rev. Lett. **77**, 5315 (1996).

[37] M. Meister, S. Arnold, D. Moll, M. Eckart, E. Kajari, M. A. Efremov, R. Walser, and W. P. Schleich, Adv. At. Mol. Opt. Phys. **66**, 375 (2017).

[38] A. L. Fetter, J. Low Temp. Phys. **106**, 643 (1997).

[39] A. L. Fetter and D. L. Feder, Phys. Rev. A **58**, 3185 (1998).

[40] A. Muñoz Mateo and V. Delgado, Phys. Rev. A **74**, 065602 (2006).

[41] A. Muñoz Mateo and V. Delgado, Phys. Rev. A **75**, 063610 (2007).

[42] A. Muñoz Mateo and V. Delgado, Phys. Rev. A **77**, 013617 (2008).

[43] A. Nicolin and R. Carretero-González, Physica A **387**, 6032 (2008).

[44] A. O. Jamison, J. N. Kutz, and S. Gupta, Phys. Rev. A **84**, 043643 (2011).

[45] Y. Margalit, Z. Zhou, S. Machluf, Y. Japha, S. Moukouri, and R. Folman, New J. Phys. **21**, 073040 (2019).

[46] M. Keil, S. Machluf, Y. Margalit, Zh. Zhou, O. Amit, O. Dobkowski, Y. Japha, S. Moukouri, D. Rohrlich, Z. Binstock *et al.*, in *Molecular Beams in Physics and Chemistry* (Springer, Cham, 2021), pp. 263–301.

[47] A. Fallon, R. H. Leonard, and C. A. Sackett, J. Phys. B **48**, 205301 (2015).

[48] S. Pandey, H. Mas, G. Vasilakis, and W. von Klitzing, Phys. Rev. Lett. **126**, 170402 (2021)

[49] A. Roura, W. Zeller, and W. P. Schleich, New J. Phys. **16**, 123012 (2014).

[50] B.-G. Englert, J. Schwinger, and M. O. Scully, Found. Phys. **18**, 1045 (1988).

[51] J. Schwinger, M. O. Scully, and B.-G. Englert, Z. Phys. D **10**, 135 (1988).
[52] M. O. Scully, B.-G. Englert, and J. Schwinger, Phys. Rev. A **40**, 1775 (1989).
[53] M. Olshanii, Phys. Rev. Lett. **81**, 938 (1998).
[54] D. S. Petrov, G. V. Shlyapnikov, and J. T. M. Walraven, Phys. Rev. Lett. **85**, 3745 (2000).
[55] F. Gerbier, Europhys. Lett. **66**, 771 (2004).
[56] T. Kinoshita, T. Wenger, and D. S. Weiss, Science **305**, 1125 (2004).
[57] S. Abend, M. Gebbe, M. Gersemann, H. Ahlers, H. Müntinga, E. Giese, N. Gaaloul, C. Schubert, C. Lämmerzahl, W. Ertmer *et al.*, Phys. Rev. Lett. **117**, 203003 (2016).
[58] K. Bongs, R. Launay, and M. A. Kasevich, Appl. Phys. B **84**, 599 (2006).